AGU PUBLICATIONS

JGR

Journal of Geophysical Research: Oceans

RESEARCH ARTICLE

10.1002/2017JC012894

Near-surface salinity and temperature structure observed with dual-sensor drifters in the subtropical South Pacific

Shenfu Dong[1], Denis Volkov[1,2], Gustavo Goni[1], Rick Lumpkin[1], and Gregory R. Foltz[1]

[1]National Oceanic and Atmospheric Administration/Atlantic Oceanographic and Meteorological Laboratory, Miami, Florida, USA, [2]Cooperative Institute for Marine and Atmospheric Studies, University of Miami, Miami, Florida, USA

Key Points:
- Regional salinity differences between 0.2 and 5 m depths are small, and Aquarius-Argo differences are not due to surface stratification
- Winds strongly modulate the surface stratification under rainfall and intense warming conditions
- A diurnal cycle of salinity is observed at 0.2 m dominated by events with winds less than 2 m/s

Correspondence to:
S. Dong,
shenfu.dong@noaa.gov

Citation:
Dong, S., D. Volkov, G. Goni, R. Lumpkin, and G. R. Foltz (2017), Near-surface salinity and temperature structure observed with dual-sensor drifters in the subtropical South Pacific, *J. Geophys. Res. Oceans, 122*, doi:10.1002/2017JC012894.

Received 16 MAR 2017
Accepted 27 JUN 2017
Accepted article online 5 JUL 2017

Abstract Three surface drifters equipped with temperature and salinity sensors at 0.2 and 5 m depths were deployed in April/May 2015 in the subtropical South Pacific with the objective of measuring near-surface salinity differences seen by satellite and in situ sensors and examining the causes of these differences. Measurements from these drifters indicate that water at a depth of 0.2 m is about 0.013 psu fresher than at 5 m and about 0.024°C warmer. Events with large temperature and salinity differences between the two depths are caused by anomalies in surface freshwater and heat fluxes, modulated by wind. While surface freshening and cooling occurs during rainfall events, surface salinification is generally observed under weak wind conditions ($\leq$4 m/s). Further examination of the drifter measurements demonstrates that (i) the amount of surface freshening and strength of the vertical salinity gradient heavily depend on wind speed during rain events, (ii) salinity differences between 0.2 and 5 m are positively correlated with the corresponding temperature differences for cases with surface salinification, and (iii) temperature exhibits a diurnal cycle at both depths, whereas the diurnal cycle of salinity is observed only at 0.2 m when the wind speed is less than 6 m/s. The amplitudes of the diurnal cycles of temperature at both depths decrease with increasing wind speed. The mean diurnal cycle of surface salinity is dominated by events with winds less than 2 m/s.

1. Introduction

Temperature, salinity, and pressure together determine the density of seawater, which plays a fundamental role in ocean circulation. Temperature data have been collected for a longer period of time compared to salinity. In particular, since the 1980s satellite observations have provided global sea surface temperature fields on a daily basis, enabling crucial advancements to our understanding of the Earth's climate system. In contrast, measurements of ocean salinity were limited until the initiation of the Argo project in 2000. Sea surface salinity (SSS) observations from space became available only in recent years thanks to three satellite missions: SMOS (Soil Moisture and Ocean Salinity) launched in November 2009 [*Kerr et al*., 2010]; Aquarius SAC-D launched in June 2011 [*Lagerloef et al*., 2008] and operated until June 2015; and SMAP (Soil Moisture Active Passive) launched in January 2015 [*Fore et al*., 2016]. The satellite salinity missions were motivated in large part by the idea that SSS is a potential indicator of changes in the global water cycle [*Gordon and Giulivi*, 2008; *Rhein et al*., 2013]. Application of satellite SSS measurements in climate research will not only advance our knowledge of the global climate system, but will also provide a test bed for its capabilities and utility for oceanographic studies, such as deep water formation at high latitudes.

Satellite SSS retrievals have improved significantly over the past few years [*Melnichenko et al*., 2016]. The large-scale spatial structure of SSS from Aquarius averaged over a 3-year period (2012–2014) (Figure 1a) [*Lagerloef et al*., 2015] is similar to the near-surface salinity observed over the same period by Argo profiling floats (Figure 1b) [*Roemmich and Gilson*, 2009]. However, differences can be as large as $\pm$0.5 psu in some regions (Figure 1c). Substantial differences in temporal evolution are also shown in regionally averaged time series in the subtropical South Pacific (Figure 1d). To maximize the value of satellite SSS retrievals, it is important to understand the cause of these differences. Comparing satellite SSS retrievals with in situ near-surface salinity measurements is fundamental for evaluating the accuracy of remote sensing products and for improving retrieval algorithms. However, the direct comparison is challenged by the fact that the two types of measurements are usually taken at different depths and can be different if vertical stratification exists between the two measurement depths. The microwave radiometers on satellites measure the skin

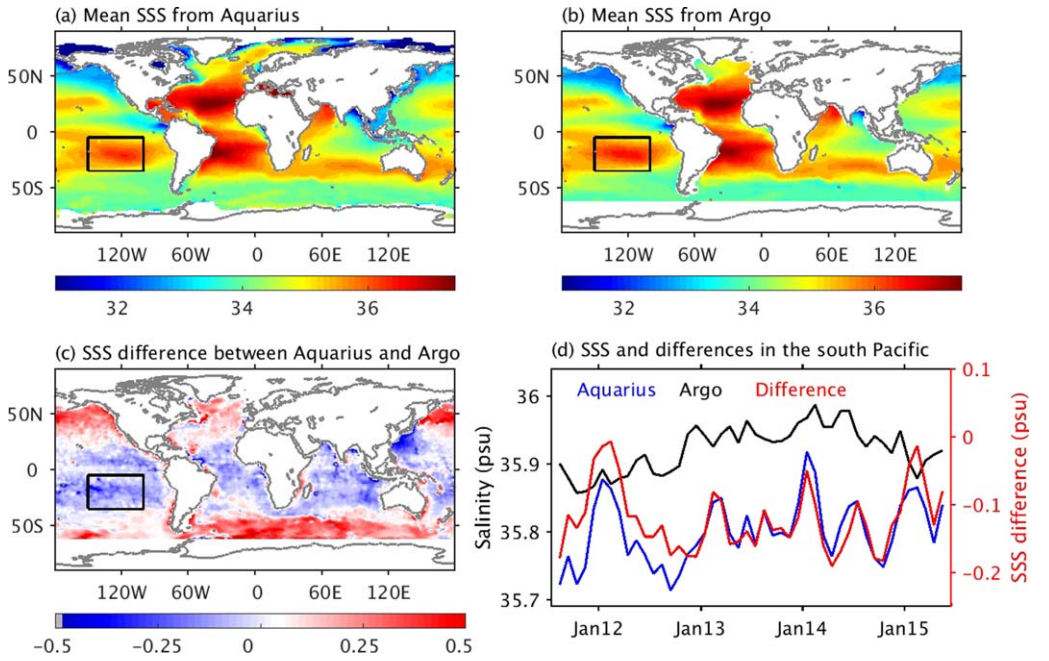

Figure 1. Three year (2012–2014) mean sea surface salinity from (a) Aquarius and (b) Argo monthly maps. (c) Mean difference of the sea surface salinity between Aquarius and Argo. (d) Time series of sea surface salinity averaged over the region of salinity maximum in the subtropical South Pacific from Aquarius (blue), Argo floats (black), and their differences (red). The monthly salinity maps used are the version 4.0 Aquarius data from PO.DAAC and the gridded Argo data from Scripps Institution of Oceanography.

salinity at a depth of ∼1 cm, whereas the in situ near-surface salinity is measured by Argo floats at depths between 1 and 5 m. Unlike the extensive studies of the vertical stratification of temperature in the upper few meters of the ocean during the past few decades [e.g., *Fairall et al*., 1996; *Wick et al*., 1996; *Murray et al*., 2000; *Donlon et al*., 2002, 2005], studies of the near-surface salinity structure were initiated only in recent years, mostly motivated by the analysis of satellite salinity data [*Boutin et al*., 2016, and references therein]. Improving our knowledge of the salinity structure in the upper few meters of the ocean is crucial for understanding, interpreting, and assessing the differences between satellite and in situ SSS measurements.

It has been reported that the upper few meters of the ocean are normally well mixed when the surface wind speed is above 6 m/s [e.g., *Murray et al*., 2000; *Gentemann et al*., 2004]. However, under weak wind conditions vertical salinity stratification can develop due to precipitation and evaporation. Precipitation leads to freshening at the surface and, therefore, generates stable vertical salinity stratification in the top few meters. Evaporation has the opposite effect by removing freshwater from the surface and, thus, increasing surface salinity and creating salinity stratification that by itself is unstable. Because of its stability, the precipitation-generated fresher surface layer tends to last longer, whereas the evaporation-generated saltier layer tends to be mixed rapidly. Previous studies [*Zhang and Zhang*, 2012; *Yu*, 2010] based on theoretical models have suggested that the ocean haline skin layer effect due to surface evaporation is between 0.05 and 0.3 psu. The thickness of the haline skin layer is usually less than 0.1 mm, much thinner than the microwave penetration depth of 1 cm. Therefore, the impact of haline skin layers on satellite salinity is estimated to be negligible ($<$0.01 psu). Also, it is extremely difficult to measure salinity at a depth of 0.1 mm with currently available in situ instruments. As a result, the majority of recent studies were focused on understanding the vertical stratification due to rain-induced surface freshening and its impact on the differences between satellite retrievals and in situ measurements [*Boutin et al*., 2016, and references therein].

Rain-induced surface freshening in the upper 2 m can be large, in some cases exceeding 1 psu [*Anderson and Riser*, 2014; *Drushka et al*., 2016]. In regions with frequent rainfall, vertical stratification can contribute to the differences between satellite SSS and in situ near-surface salinity measurements [*Boutin et al*., 2013; *Drushka et al*., 2016]. The relationship between rain rate and salinity differences between satellite and in situ measurements was quantified in several recent studies [e.g., *Boutin et al*., 2014; *Drucker and Riser*, 2014; *Meissner et al*., 2014; *Drushka et al*., 2016]. These studies showed that individual rain events can generate

strong near-surface salinity stratification. However, these events are extremely patchy, sparse in space and time, and are accompanied by a wide range of ocean conditions. On average, the dependence of the satellite-Argo salinity difference on rain rate was found to be around 0.1–0.2 psu/(mm/h). Direct measurements of salinity and winds have shown that surface stratification also inversely depends on wind speed [*Asher et al*., 2014; *Drushka et al*., 2016], with stronger winds tending to mix the freshwater input deeper and decrease the stratification, and vice versa. Adding to the complexity of the freshening events, several studies [*Back and Bretherton*, 2005; *Raymond et al*., 2009] have demonstrated that the strength of precipitation and wind speed are highly correlated, with more precipitation usually associated with stronger winds.

In addition to the different measurement depths, the direct comparison of satellite and in situ measurements is challenged by their different spatial and temporal sampling. Satellite salinity measurements represent spatial averages over the satellite's footprint (40–150 km), whereas in situ measurements represent single point values. The sun-synchronous satellite missions measure salinity at nearly fixed times with a local equator-crossing time of 6:00 (descending) and 18:00 (ascending). In situ salinity measurements are distributed more evenly throughout the day. Previous studies [*Cronin and McPhaden*, 1999; *Drushka et al*., 2014] using mooring measurements in the tropics showed that SSS experiences diurnal variations. Therefore, the sampling differences may result in significant differences in regions with large spatial or temporal variability. Hence, it is still not clear how much the actual surface salinity stratification contributes to the differences seen between satellite and in situ measurements, and what portion of those differences is due to different spatial and temporal sampling.

Simultaneous measurements of salinity at depths corresponding to the microwave penetration depth (∼1 cm) and in situ measurement depth (∼1–5 m) are critical to further advance our understanding of the processes responsible for satellite-in situ salinity differences, and to analyze and interpret satellite salinity data. Different platforms [*Boutin et al*., 2016] have recently been used to measure the near-surface salinity and near-surface salinity stratification, including the Surface Salinity Profiler [*Asher et al*., 2014], Wave Glider [*Hodges and Fratantoni*, 2014], and surface temperature and salinity (STS)-Argo float [*Anderson and Riser*, 2014]. These platforms have been used to observe rain-induced freshening in the tropics during short time periods. In an effort to assess salinity differences at two depths close to the satellite and in situ measurements over a wide range of ocean conditions, surface drifters with dual temperature and salinity sensors were designed for this study to simultaneously measure salinity and temperature at approximately 0.2 and 5 m depths. This allows us to directly observe the near-surface salinity gradient and assess the effect of the near-surface salinity stratification on the differences between satellite and in situ SSS.

The characteristics and specifications of the drifters designed to explore the salinity differences at the two depths close to the satellite and in situ measurements are described in section 2. Section 2 also includes description of the drifter deployments and measurements as well as other data used in this study. Section 3 shows the salinity and temperature differences at the two measurement depths. Section 4 describes the diurnal cycles of temperature and salinity observed by the drifters. Section 5 summarizes the main conclusions.

2. Data and Methods

2.1. Dual-Sensor Drifters

The drifters used in our experiments are manufactured by Pacific Gyre Inc. (http://www.pacificgyre.com) and represent an upgraded version of those deployed during the first SPURS (Salinity Processes in the Upper Ocean Regional Study) campaign [*Centurioni et al*., 2015; *Hormann et al*., 2015]. The unique aspect of our drifters is that they are equipped with two pairs of conductivity and temperature sensors, positioned at depths of 0.2 m and 5 m. The original version of Surface Velocity Program (SVP) drifters with a larger surface float (41 cm in diameter) and drogue (91 cm long) is used for these dual-sensor drifters, with the drogue sized to maintain the same drag area ratio as standard SVP-type drifters. The upper conductivity and temperature sensors (Sea-Bird Electronics SBE37-SI) are mounted at the bottom of the float (∼0.2 m) to avoid direct radiative heating. The other pair of sensors (SBE37-IM) is mounted on the tether at 5 m depth, above the drogue. The accuracy of both SBE37-SI and SBE37-IM instruments is 0.0003 S m^{-1} for conductivity (∼0.003 psu) and 0.002°C for temperature. Details of the sensors and sampling strategy are described in *Hormann et al.* [2015]. These drifters collect data every 30 min, therefore resolving diurnal changes and

providing high spatiotemporal resolution time series. Although differences in salinity between depths of 0.2 m and 1 cm (i.e., the satellite measurement depth) are anticipated, measurements from the dual-sensor drifters will provide a data set more suited to validate satellite SSS retrievals compared to measurements of bulk SSS at 1 or 5 m. The drifter data will also help to identify the contributions from biases in satellite retrievals and small-scale variations of SSS due to weather events on salinity differences between Aquarius and Argo (Figure 1), which is important for future improvement of the retrieval algorithm.

Twelve dual-sensor drifters have been deployed in three different regions: the subtropical South Pacific (three drifters deployed in April–May 2015), the Southern Ocean (three drifters deployed in December 2015), and the eastern tropical Pacific (six drifters deployed in August–September 2016, *Volkov et al.* [2017]). These regions were chosen because they exhibit relatively large salinity differences between Aquarius and Argo, and the salinity differences exhibit strong variability. In addition, wind speed in the subtropical South Pacific and in the eastern tropical Pacific is weak and, therefore, surface stratification in these regions is expected to be stronger. Finally, and most importantly, these regions experience different weather conditions and are dynamically different; therefore, the potential factors contributing to surface salinity stratification are expected to be different in each region. The subtropical regions experience relatively strong evaporation, which could induce a saltier skin layer, resulting in positive values in surface salinity difference between Aquarius and Argo. However, salinity from Aquarius in the subtropical South Pacific was fresher than salinity from Argo data (Figure 1d), suggesting that other processes may determine the differences. The tropical Pacific experiences strong precipitation, which could generate a fresher skin layer. This may contribute to the negative values in surface salinity differences between Aquarius and Argo in this region (Figure 1c). Because the Southern Ocean experiences strong winds, the top few meters of the ocean are expected to be well mixed. However, salinity values obtained from Aquarius were higher than salinity from Argo, which may be due to satellite retrieval errors at higher latitudes. In this study, we present results from the three drifters deployed in the subtropical South Pacific. Analysis of data from the other two regions is ongoing and will be presented in separate studies.

2.2. Drifter Data Processing

Three drifters, each equipped with two temperature and salinity sensors, were deployed in April–May 2015 in the high salinity region of the subtropical South Pacific (Figure 2). The first drifter was deployed at the northern boundary of the high salinity region (8.8°S, 109.9°W, drifter A) on 10 April and drifted into the center of the high salinity region after 5 months. The other two drifters were deployed close to the salinity maximum in mid-May at 20.3°S, 115.1°W (drifter B) and 25.5°S, 125.1°W (drifter C). Because the surface currents and winds are usually weak in this region, these drifters remained close to their initial deployment locations (Figure 2). Unfortunately, after ~130 days of deployment (18 August 2016), the salinity measurements from the drifter A became contaminated (Figure 3a) probably by particles stuck in the conductivity sensors. Although the salinity differences between the two depths reduced to ±0.3 psu at the beginning of 2016, the values were still too large compared to the measurements from the other two drifters (Figures 3b and 3c). Therefore, salinity data from drifter A after 18 August 2016 are excluded in the analysis presented in this study.

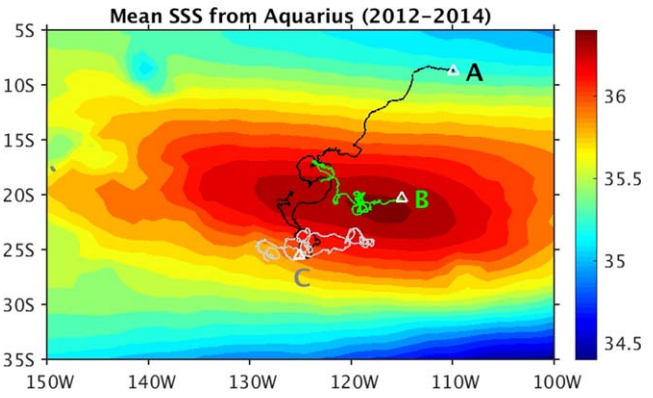

Figure 2. Trajectories of the three dual-sensor drifters deployed during April/May 2015 in the subtropical South Pacific. The color shading shows the 3 year (2012–2014) averaged SSS from Aquarius gridded monthly maps (version 4.0 from PO.DAAC). Unit is psu.

As discussed in *Hormann et al.* [2015] and *Reverdin et al.* [2014], large fresh biases in the salinity measurements occasionally occur, due to the presence of air bubbles or objects stuck in the conductivity cell. Following *Reverdin et al.* [2014], isolated large biases (exceeding 0.1 psu from two adjacent measurements) at both 0.2 and 5 m depths are removed. Longer periods (>5 days) of fresh biases are also observed at 0.2 m depth from drifter B during May–July 2016 (Figure 3a). Those biases are manually removed. In

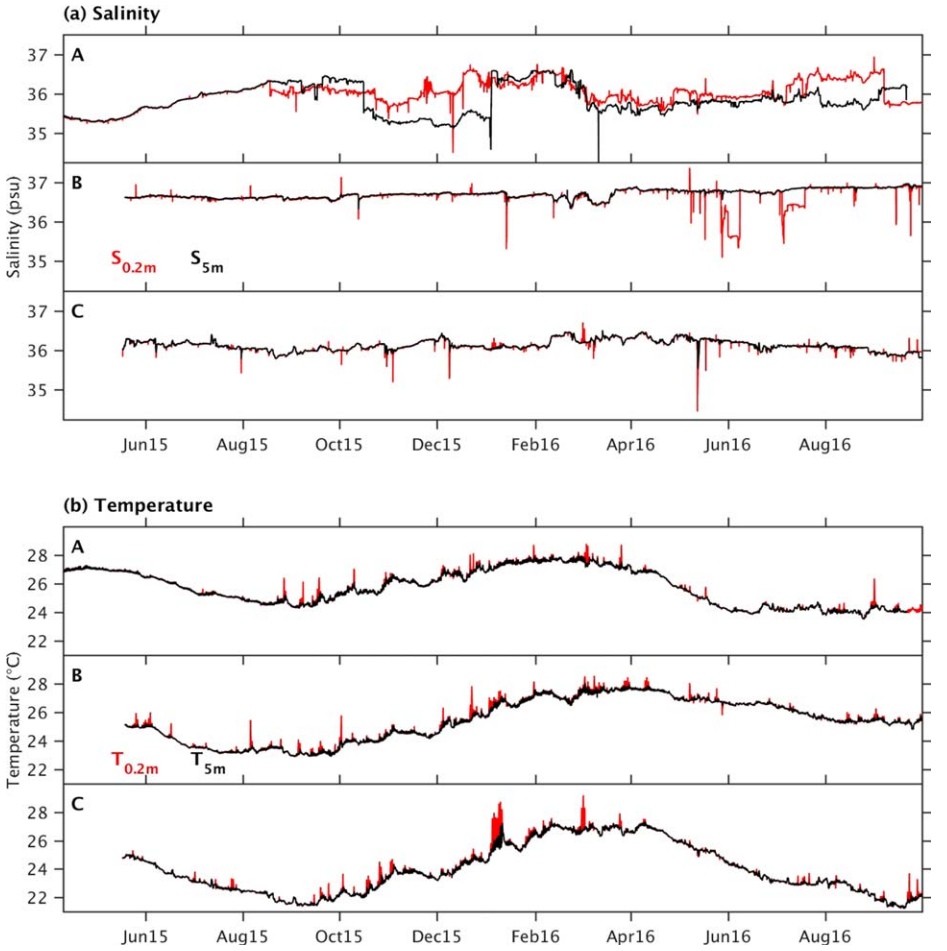

Figure 3. Time series of (a) salinity and (b) temperature from the three drifters (A, B, and C) shown in Figure 2, with values at 0.2 m shown as red and values at 5 m shown as black.

addition to the large biases, the salinity differences between 0.2 and 5 m measurements ($\Delta S = S_{0.2m} - S_{5m}$) from drifters B and C increase from the beginning of 2016 due to drift in one or both of the conductivity sensors. To remove the drift in ΔS, 30 day running averages of ΔS were performed. The departures of the low-pass filtered ΔS from the 2015 average ΔS were removed from the salinity measurements at 0.2 m beginning on 1 January 2016. We note that our attempts to determine which sensor drifted, through comparisons to collocated Argo float data, were unsuccessful because the differences between salinities from drifters and the collocated Argo surface measurements (within $\pm 1°$ latitude/longitude and ± 1.0 h) can be as large as 0.4 psu, which is well above the difference ($\sim$0.15 psu) between the two conductivity sensors. Because the analyses presented in this study are focused on the salinity differences, removing the drift either from $S_{0.2m}$ or S_{5m} will not affect the results.

Standard errors given in the following analyses are calculated based on the degrees of freedom determined for the corresponding variables using the first zero crossing of the autocorrelation function.

2.3. Atmospheric Data Products

In order to investigate the processes that contribute to changes in the near-surface temperature and salinity, we also used surface wind speed, precipitation, solar radiation, evaporation, specific humidity, and skin temperature from the Modern-Era Retrospective Analysis for Research and Application version 2 (MERRA-2) product [*Molod et al.*, 2015]. MERRA-2 data are derived from the Goddard Earth Observing System version 5 (GEOS-5) data assimilation system and are available on a 0.5 $\times$ 0.625 spatial grid and 1 h temporal resolution. In addition, we used precipitation data from the Tropical Rainfall Measuring Mission (TRMM)—a joint NASA and Japan Aerospace Exploration Agency mission [*Huffman et al.*, 2007]. The gridded TRMM

precipitation data from the Goddard Distributed Active Archive Center (GES DISC DAAC) are on a 3 h temporal and 0.25 × 0.25 spatial resolution. The gridded MERRA-2 and TRMM products were linearly interpolated to the locations and times of the drifter measurements.

3. Salinity and Temperature Differences Between 0.2 and 5 m Depth

The time series of salinity and temperature from the three drifters deployed in the subtropical South Pacific are shown in Figure 3. The salinity from the two drifters deployed at 20°S and 25°S do not show much variability during the 17 month observational period, with time-mean values of 36.70 psu and 36.13 psu and standard deviations of 0.11 psu and 0.13 psu, respectively (Figure 3a). The temperature measurements from all three drifters (Figure 3b) are dominated by the seasonal cycle, although to some extent the spatial variations may contribute to the observed changes.

3.1. Salinity Differences

The salinity differences between 0.2 and 5 m depth ($\Delta S = S_{0.2m} - S_{5m}$) are very small, except during periods with strong rainfall or weak winds, which will be discussed later. The overall average of ΔS is −0.013 psu with standard error of 0.002 psu, indicating that the water at 0.2 m depth is slightly fresher than that at 5 m depth. Figure 4a shows the histogram of the salinity differences. It is very clear that for the majority of the time during the study period (83.4%), $S_{0.2m}$ is fresher than S_{5m}. However, the differences are well below the 0.2 psu accuracy of the Aquarius mission and the mean difference (−0.13 psu) between the Aquarius and Argo float gridded products in the study region. Consistent with previous studies [e.g., *Anderson and Riser*, 2014], the drifter measurements suggest that the differences between the gridded products from Argo floats and Aquarius are not due to surface salinity stratification.

Although the mean salinity difference between the two measurement depths is very small, ΔS varies in a large range from −1.72 psu to +0.60 psu. Large values of ΔS ($|\Delta S| > 0.1$ psu) account for only 1.3% of the total measurements, and more than 97.7% of the differences are within ±0.05 psu. The large differences between $S_{0.2m}$ and S_{5m} ($|\Delta S|>0.1$) are dominated by negative values, i.e., water at 0.2 m depth is fresher than that at 5 m depth. The observed freshening cases correspond well to rainfall events (Figures 5a and 5b), as has been reported in previous studies [*Boutin et al.*, 2013, 2014; *Anderson and Riser*, 2014; *Meissner et al.*, 2014]. However, in contrast to the previously reported linear dependence of the satellite-Argo salinity differences on rain rate, results obtained here (Figure 5c) suggest that the salinity differences and rainfall do not have a linear relationship. The large differences occur mostly when the rainfall is below 2 mm/h. This is most likely due to the fact that strong rain events (>2 mm/h) are accompanied by stronger winds (>6 m/s) (Figure 5d): for the cases with rain rate above 2 mm/h, 92% of the time the winds exceed 6 m/s. This results in stronger mixing and, therefore, reduced stratification in the near-surface layer. However, it should be

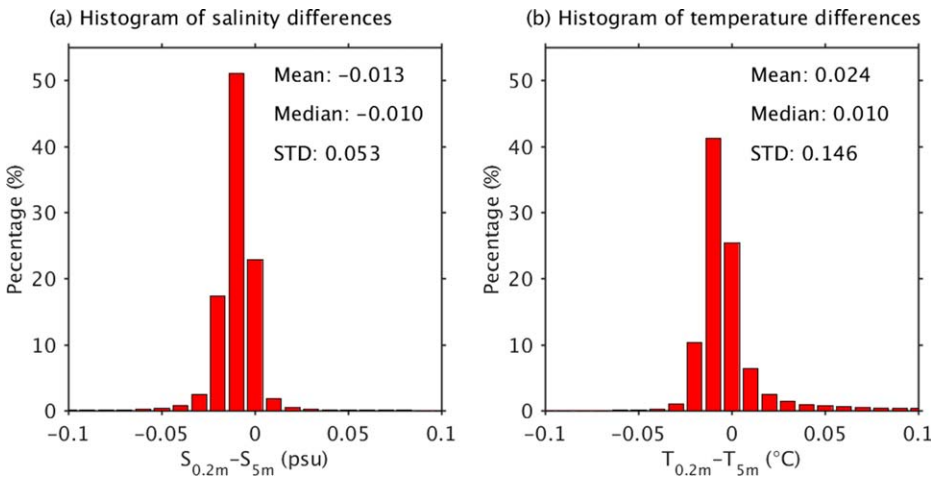

Figure 4. Histogram of (a) salinity differences ($S_{0.2m} - S_{5m}$) and (b) temperature differences ($T_{0.2m} - T_{5m}$) using data from all three drifters. The values of the time-mean, the median, and the standard deviation of the differences are given. Units are °C for temperature and psu for salinity.

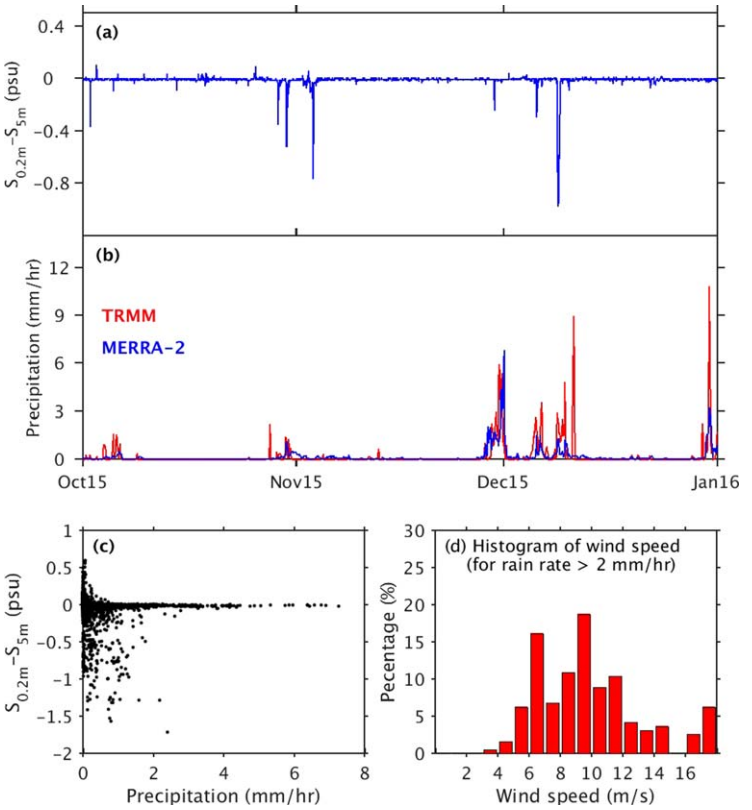

Figure 5. (a) Salinity differences ($S_{0.2m} - S_{5m}$) from the drifter deployed near 25°S during a 3 month period (October–December 2015), and (b) the corresponding precipitation from TRMM (red) and MERRA-2 (blue). (c) Scatterplot of the salinity differences against MERRA-2 precipitation for data from all three drifters (drifter A, B, and C) during our study period. (d) Histogram of wind speeds for cases with rain rate exceeding 2 mm/h.

noted that other factors may also affect the relationship between the freshening and rain rate obtained here, including spatial sampling differences (i.e., point measurements from drifters versus spatial averages over satellite footprint) and noises in the MERRA-2 product.

Although negative values of ΔS (i.e., freshening events) are much more common when the magnitude of ΔS is large (Figure 5), drifter measurements also show the occurrence of large positive values of ΔS, meaning that water at 0.2 m depth is saltier than that at 5 m depth. The concurrent measurements of temperature and salinity from drifters (Figure 3) show the correspondence between surface salinification events ($S_{0.2m} > S_{5m}$) and strong surface warming ($T_{0.2m} > T_{5m}$). These strong surface warming events are closely linked to low-wind conditions, which will be discussed in section 3.3. Further examination of the drifter data indicates that large positive values of ΔS occur between 9:30 and 18:30 local time, i.e., during the warming phase of the diurnal cycle. This suggests that strong surface warming-induced stability and weak mixing under low-wind conditions allow the development of unstable surface salinity stratification (high salinity at 0.2 m than 5 m). Our results suggest that the magnitude of surface salinification depends on both winds and insolation (Figure 6). Large values of positive ΔS are observed mostly with winds below 4 m/s, and ΔS increases with increasing solar insolation. The wind dependence is consistent with the observed surface

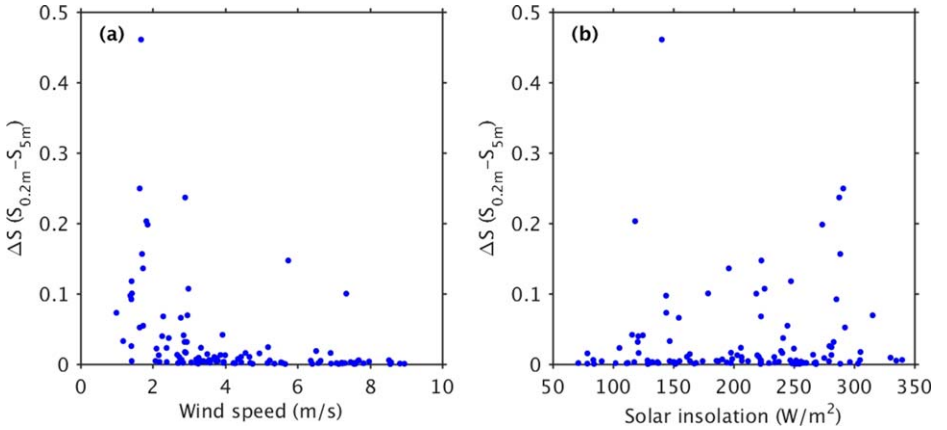

Figure 6. Scatter plots of salinity difference against (a) wind speed and (b) solar insolation for cases with surface salinification ($S_{0.2m}$ is saltier than S_{5m}).

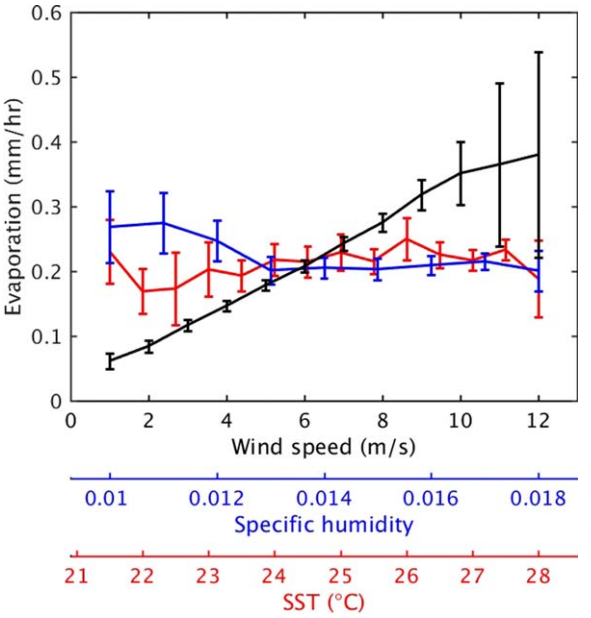

Figure 7. Changes of evaporation with wind speed (black), specific humidity (blue), and sea surface temperature (red) derived from the MERRA-2 products.

salinification in the subtropical North Atlantic during the summer of 2012 based on data from the Sub-Tropical Atlantic Surface Salinity Experiment/Salinity Processes in the Upper-ocean Regional Study (STRASSE/SPURS) cruise [*Asher et al.*, 2014]. However, in contrast to *Asher et al.* [2014], who found that surface salinification occurs when daily solar insolation exceeds 300 W/m^2, positive ΔS from the drifters occurs over a wide range of insolation (Figure 6b). These differences could be due to the seasonal variations of solar insolation and the differences in the study periods. Data presented by *Asher et al.* [2014] were collected during summertime with high solar insolation, whereas the drifter data used in this study are year-round.

As mentioned earlier, it is expected that the large positive ΔS (surface is saltier) should correspond to stronger evaporation. However, the evaporation obtained from MERRA-2 during the larger positive ΔS events is very low, with an average of 0.10 mm/h compared to an overall average of 0.22 mm/h. This is consistent with the weak mixing under low-wind conditions, which confines the effect of evaporation in a thin layer. Factors affecting evaporation include wind speed, surface temperature, and humidity. Stronger winds and higher temperatures act to increase evaporation, whereas higher humidity tends to decrease evaporation. Analysis of MERRA-2 data indicates that evaporation is highly correlated with wind speed, but not with the surface temperature and specific humidity. Figure 7 clearly shows the increase of evaporation from 0.06 mm/h to 0.35 mm/hr as wind increases from 1 to 10 m/s. For specific humidity below 0.013, evaporation decreases slightly with increasing humidity. However, MERRA-2 data do not show statistical dependence of evaporation on SST. It should be noted that because the SST in the MERRA-2 assimilation is derived from weekly OISST [*Molod et al.*, 2015], it does not resolve the diurnal cycle (not shown). Therefore, the MERRA-2 assimilation cannot capture the impact of temperature on evaporation during strong diurnal warming under calm ocean conditions. Consequently, although our analysis suggests that the weak mixing under low-wind speeds is more important than strong evaporation for generating larger positive ΔS, the model's temporal resolution of SST may be responsible for the low evaporation during the observed strong diurnal warming.

3.2. Temperature Differences

Similar to the salinity differences, the temperature differences between the two depths ($\Delta T = T_{0.2m} - T_{5m}$) are small (Figure 4b). About 53.7% of the time $T_{0.2m}$ is lower than T_{5m}, with an average difference of -0.014°C. This is likely due to the cool-skin effect related to the upward heat flux at the sea surface. Because of the diurnal warming effect, the majority (89%) of the negative ΔT values occur after 16:00 and before 8:00 local time. About 97% of the surface cooling is less than 0.03°C. Only 0.5% of the negative ΔT is smaller than -0.1°C, with the largest negative ΔT being about -0.85°C. These large negative values are accompanied by large negative values of ΔS, suggesting that the stronger near-surface cooling is due to rainfall events.

In contrast, $T_{0.2m}$ is higher than T_{5m} only during 21% of the time. The largest positive ΔT is about 2.65°C with an average of 0.15°C. About 86% of the positive ΔT occurs between 8:00 and 18:00 local time, with high values of positive ΔT in general around 15:00 local time, suggesting that the positive ΔT is mostly related to diurnal warming. Because the magnitude of ΔT is greater when ΔT is positive (surface is warmer than 5 m depth), despite positive ΔT being rarer than negative ΔT, the mean ΔT is also positive (0.024°C with standard error of 0.004°C).

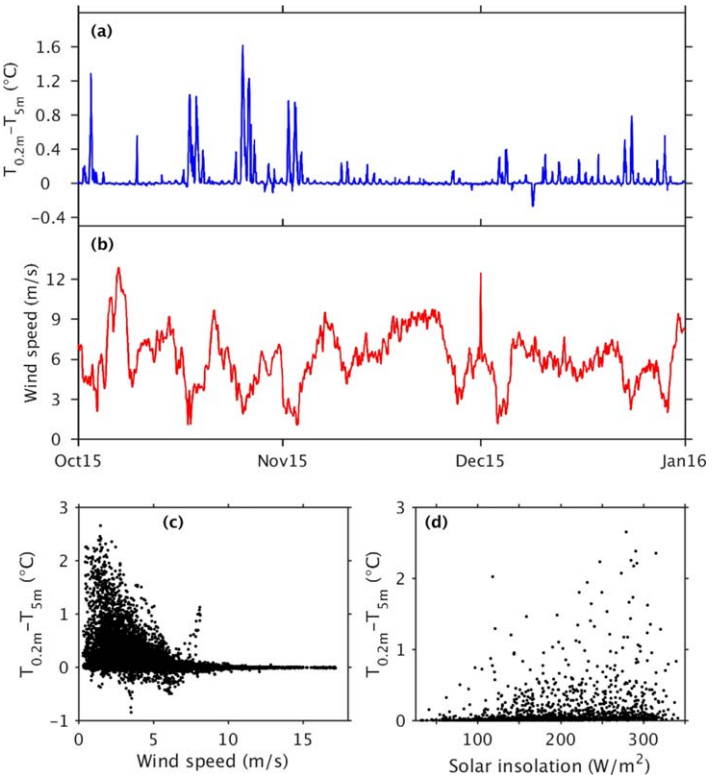

Figure 8. Similar to Figure 5 but for temperature and wind speed. (a) Temperature differences ($T_{0.2m} - T_{5m}$) from the drifter deployed near 25°S during a 3 month period (October–December 2015), and (b) the corresponding wind speed from MERRA-2. Scatterplot of the temperature differences against MERRA-2 (c) wind speeds and (d) insolation for data from all three drifters during our study period.

The two main factors influencing the temperature differences are wind and solar insolation (Figures 8c and 8d), which are discussed in the following sections. In general, surface stratification occurs mostly when surface winds are below 6 m/s (Figure 8c), and ΔT increases with increasing solar insolation (Figure 8d).

3.3. Wind Impact on ΔT and ΔS

Numerous studies [e.g., *Murray et al.*, 2000; *Donlon et al.*, 2002; *Gentemann et al.*, 2004; *Dong et al.*, 2006] have found that near-surface temperature gradients occur predominantly during periods with weak winds, whereas stronger winds effectively mix the water column. Consistent with previous studies, the impact of wind speed on temperature differences is clearly seen in Figures 8a and 8b, with large values of ΔT corresponding to low-wind speeds. The scatter plot of wind speed from MERRA-2 and temperature differences from all three drifters (Figure 8c) shows that ΔT decreases rapidly with increasing wind speed in the range ~0–6 m/s. The impact of wind speed on ΔS is not as obvious as for ΔT, and the scatter plot of ΔS against wind speed (not shown) is quite noisy. However, it does indicate that the largest values of ΔS occur when the wind is weak.

The low-wind effect is clearly demonstrated during 4–10 January 2016 when the wind speed remained below 3 m/s for nearly the entire 7 day duration of the drifter's track close to 25°S (Figures 9a–9c). As a result of the low wind, ΔT is positive throughout this period, even at nighttime when the surface is usually cooler than the subsurface due to heat loss to the atmosphere. The 7 day averaged ΔT is about 1.12°C, well above the overall average value of 0.02°C. The continuous low-wind conditions also had a strong impact on the near-surface salinity stratification. Compared to the entire 17 month period, during which only 2% of the data have a positive ΔS, 57% of the ΔS values during this 1 week period were positive. Figures 9d–9f show another example of the low-wind effect for the same drifter during a 3 day period nearly 2 months later (29 February to 2 March 2016). The surface salinification during this low-wind event was even more clearly demonstrated. Low wind exerts two competing effects on the development of surface salinification. On one hand, reduced evaporation during weak winds decreases surface salinification. On the other hand, weak mixing under low-wind conditions favors surface salinification. The strengthened surface salinification during periods of low wind (Figure 9) suggests that the direct wind mixing effect plays a larger role in generating unstable salinity stratification.

The lack of a significant statistical relationship between precipitation and surface freshening can also be attributed to the effect of wind speed. Because of strong mixing during high winds, even with large precipitation the freshwater input will be distributed within a relatively thick layer and, therefore, surface freshening as well as the near-surface salinity gradient are likely to be quite small. On the contrary, during weak winds, the freshwater input is confined to a thinner layer, which in turn will induce strong surface freshening and a large near-surface salinity gradient. The examples shown in Figure 10 clearly demonstrate these scenarios. The precipitation event for the 2016 case (Figures 10e–10h) is somewhat weaker and shorter-

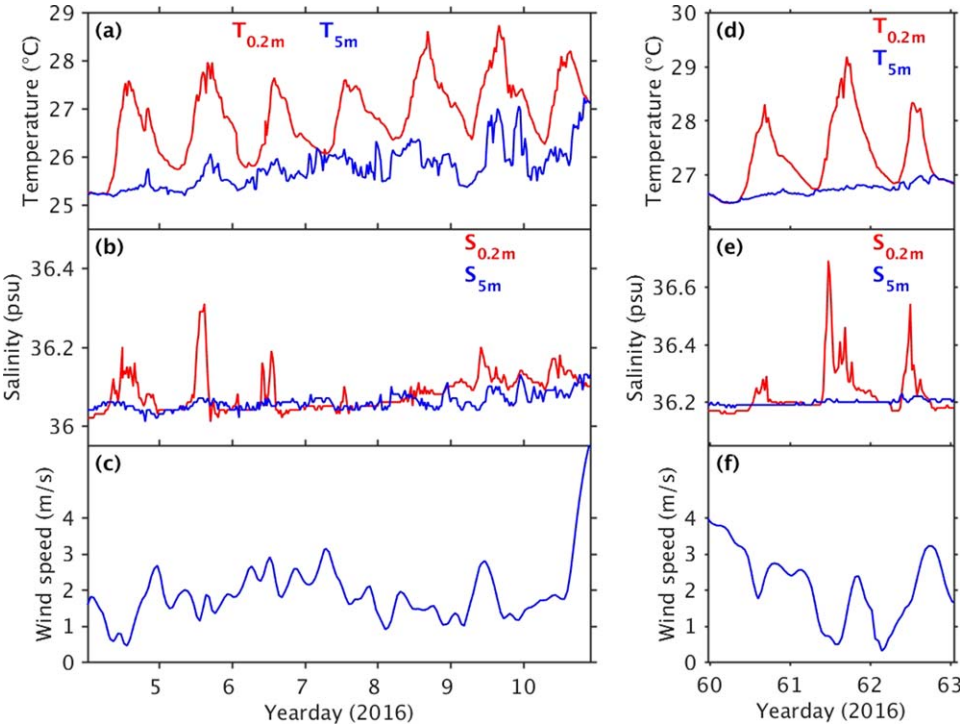

Figure 9. Examples of low-wind impact on temperature and salinity during two periods in 2016 from drifter at 25°S. (a) Temperature, (b) salinity, and (c) wind speed during 4–10 January 2016. (d and e) similar to (a and c), but for the period 29 February to 2 March 2016. The values for temperature and salinity at 0.2 m depth are shown in red and the values for 5 m depth shown in blue. Units are °C for temperature, psu for salinity, and m/s for wind speed.

lived compared to the 2015 case (Figures 10a–10d). However, the winds are much weaker during the 2016 case, and as a result the near-surface freshening for this case is much stronger and the salinity differences between 0.2 and 5 m are larger. The response of surface cooling to wind speed during precipitation events (Figures 10b and 10f) is very similar to that of the surface freshening, i.e., weak and deep-reaching cooling during strong winds, and strong and surface-confined cooling during weak winds. Consistent with the results for positive ΔS where low winds (weak mixing) play a larger role in generating large positive ΔS, low winds are more important than strong rainfall for large negative ΔS development.

It is interesting to note that during freshening events the near-surface salinity decreases to a minimum in a rather short time period, generally within 1–2 h, but the recovery process takes longer, from a few hours to 1 day.

3.4. Relationship Between ΔS and ΔT

The concurrent temperature and salinity data provide an opportunity to explore whether there is a relationship between the salinity and temperature differences. Considering extensive studies in the past that have advanced our understanding of the near-surface temperature structure, a possible link between temperature structure and salinity structure will lead to a better characterization of the near-surface salinity structure and ultimately contribute to future improvements in satellite retrieval algorithms.

The input of cold and freshwater during rain events induces freshening and cooling at the same time, and the vertical structures of the freshening and cooling are influenced by the wind speed. When there is strong surface warming, winds are normally weak. Therefore, the unstable surface salinification can develop due to strong thermal stability and weak mixing [e.g., *Grodsky et al*., 2008]. Therefore, it is expected that in these cases the near-surface salinity gradient and temperature gradient should be positively correlated. Indeed, the measurements from the drifters (Figure 3) demonstrate the correspondence for extreme cases, with high salinity at the surface ($S_{0.2m}$) always occurring when there is strong near-surface warming and strong surface freshening accompanied by surface cooling. The scatterplot of ΔS against ΔT (Figure 11) shows that ΔS tends to be more positive with increasing ΔT, whereas the larger negative values of ΔT and ΔS occur

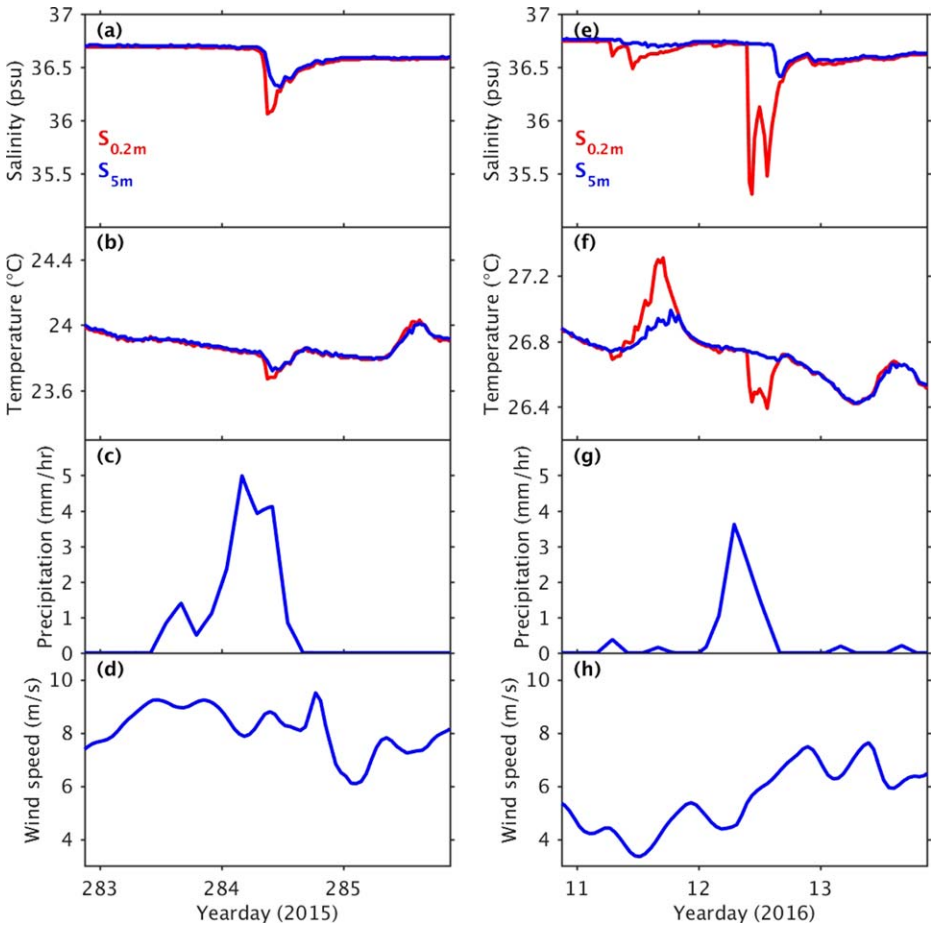

Figure 10. Examples of freshening events observed from the drifter deployed at 20°S. (a) Salinity and (b) temperature at 0.2 m (red) and 5 m (blue) depths. (c) Precipitation and (d) wind speed from MERRA-2 during the same period. (e), (f), (g), and (h) are similar to (a), (b), (c), and (d) but for another freshening event.

together. Separating the data into positive and negative ΔT, the correlation is about 0.47 for cases with positive ΔT, and 0.50 for cases with negative ΔT. Linear regression analysis suggests that, for cases with positive ΔT, a 1°C increase in ΔT corresponds to an increase in ΔS of about 0.05 $\pm$ 0.01 psu. For cases with negative ΔT, the relationship is much noisier. Those negative cases are mostly associated with rainfall events. The magnitude of rain-induced freshening and cooling is proportional to the differences in salinity and temperature between raindrop and ocean surface. Compared to the near-constant rain-ocean salinity difference ($\sim$35 psu), the rain-ocean temperature difference can vary over a large range because of variations of rain temperature. This explains the noisiness of the relationship between ΔS and ΔT. Nevertheless, linear regression analysis indicates that a 1°C decrease in ΔT corresponds to a 2.20 $\pm$ 0.05 psu decrease in ΔS. Using the averaged coefficients of thermal expansion (3.0×10^{-4}°C^{-1}) and saline contraction (7.4×10^{-4} psu^{-1}) derived from the observations of $T_{0.2m}$ and $S_{0.2m}$, the water column for both the warm/salty and cool/fresh cases in this region appears to be stable.

4. Diurnal Cycle

As pointed out in the previous section, diurnal variations of the surface temperature and salinity contribute to the differences between the two measurement depths. Unlike the extensive studies of the diurnal cycle in surface temperature [e.g., *Stommel et al.*, 1969; *Fairall et al.*, 1996; *Gille*, 2002; *Gentemann and Minnett*, 2008], the diurnal cycle in surface salinity has not been well studied because of limited observations. Previous studies of the diurnal cycle of salinity were mainly focused on the tropics using mooring data [*Cronin and McPhaden*, 1999; *Drushka et al.*, 2014]. The half-hourly data from the surface drifters provide a valuable

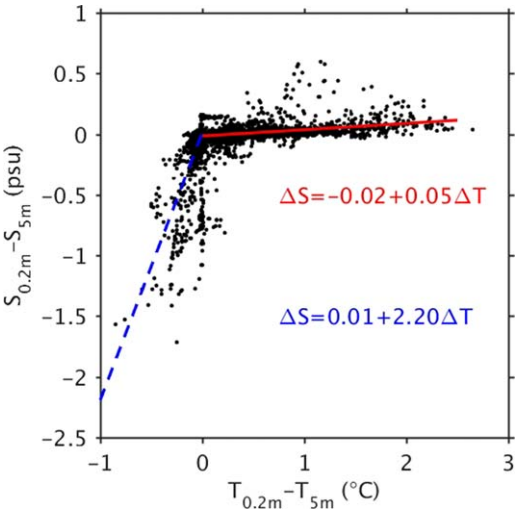

Figure 11. Scatterplot of salinity differences ($\Delta S = S_{0.2m} - .S_{5m}$) against temperature differences ($\Delta T = T_{0.2m} - .T_{5m}$). The red line is the linear regression of ΔS to ΔT for cases with $\Delta T > 0$, and the blue line for cases with $\Delta T < 0$.

data set to examine the diurnal cycle in near-surface temperature, and especially salinity, at the two measurement depths.

4.1. Time-Mean Diurnal Cycle and its Seasonality

The diurnal cycles of temperature and salinity averaged over the three drifter records are shown in Figure 12. To better demonstrate the relative values at the two measurement depths, the daily averages of T_{5m} were removed from $T_{0.2m}$ and T_{5m} for the corresponding day in deriving the diurnal cycle of temperature. The diurnal cycles of $S_{0.2m}$ and S_{5m} were derived in the same way. The temperatures at both depths show robust diurnal cycles (Figure 12a) with amplitudes of 0.23°C and 0.13°C for $T_{0.2m}$ and T_{5m}, respectively. The phase of the temperature diurnal cycle is largely controlled by daytime warming from solar radiation and nighttime cooling from longwave radiation and turbulent fluxes. At 0.2 m depth, the temperature reaches its diurnal maximum at local time 15:00 and minimum at 07:00. At 5 m depth, both the diurnal maximum and minimum occur somewhat later than those at 0.2 m depth because of the time needed for vertical flux propagation. The maximum in T_{5m} occurs at 16:30, a 1.5 h delay from the time of maximum $T_{0.2m}$, whereas the minimum T_{5m} occurs at 07:30, a half-hour delay from the time of minimum $T_{0.2m}$. Figure 12a shows that $T_{0.2m}$ is higher than T_{5m} during the day, from 08:00 to midnight, and lower than T_{5m} from midnight to 08:00 due to the cool skin effect.

To evaluate the impact of the diurnal cycle of surface temperature on evaporation, we performed a simple calculation with mean values of variables taken from MERRA-2 and drifter measurements. The diurnal anomalies in evaporation (E) due to diurnal temperature anomalies can be simplified as $\Delta E = \rho_a C_D U \Delta(q_s - q)$, where ρ_a is air density, C_D is an air-sea drag coefficient, U is the wind speed, q is specific humidity, and q_s is the specific humidity for saturated air over water at sea surface temperature ($T = \bar{T} + T'$). Here q_s is defined as $q_s = 0.622\frac{e_s}{p}$, with constant surface air pressure $p = 1013$ mb and the saturation vapor pressure a function of T, $e_s = 6.112e^{17.502T/(241+T)}$. With the mean surface temperature $\bar{T}$ of 25°C (from the three drifters) and diurnal amplitude of 0.23°C, the characteristic diurnal cycle in the specific humidity for saturated air q_s is about 2.74×10^{-4} with a mean value of 0.0196. Using the characteristic $\rho_a = 1.18$ kg/m^3 at $T = 25$°C, $C_D = 0.001$, $q = 0.0144$, and $U = 6$ m/s from MERRA-2, the diurnal amplitude in evaporation ΔE becomes 0.007 mm/h, and

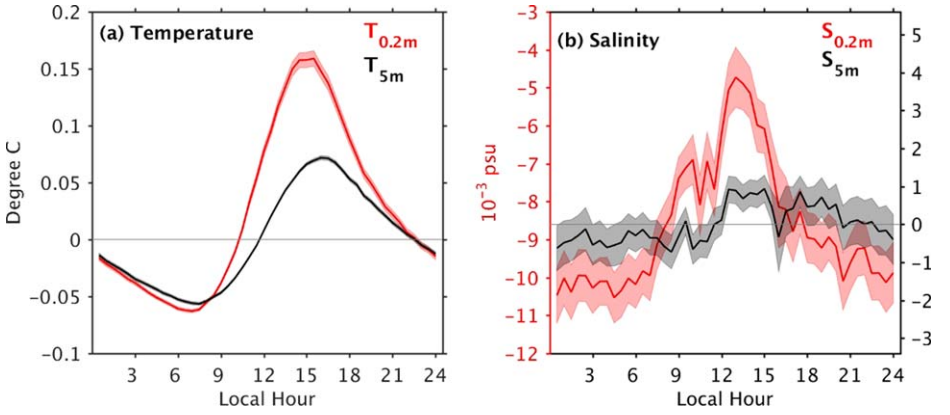

Figure 12. Diurnal cycle of (a) temperature and (b) salinity at 0.2 m (red) and 5 m (black) depths averaged over all data from the three dual-sensor drifters. Daily averages of T_{5m} and S_{5m} were removed from temperature and salinity records at both depths, respectively. Different y-axes are used for $S_{0.2m}$ and S_{5m} (b) because the mean ΔS is larger than the diurnal amplitude. The shading shows two standard errors for the corresponding variables.

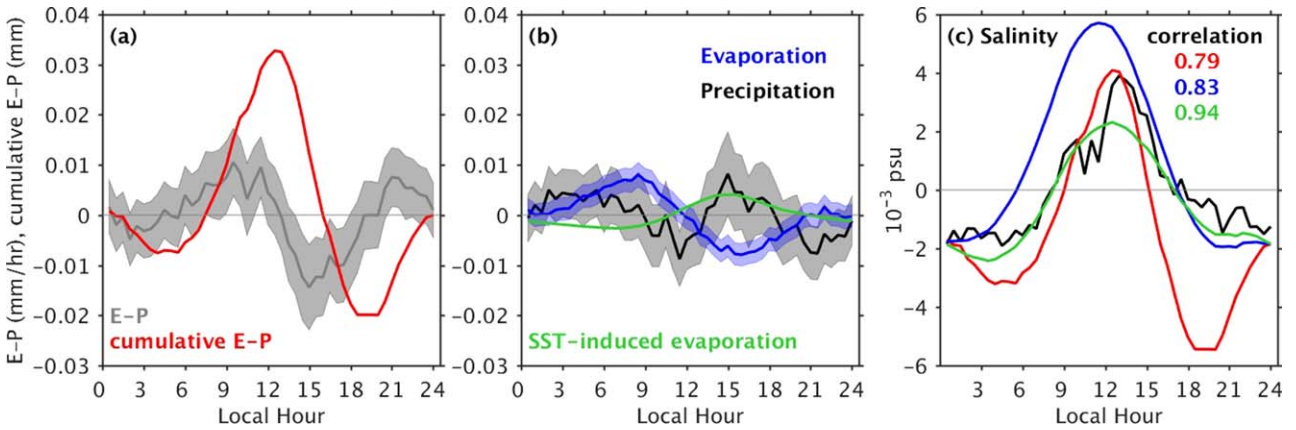

Figure 13. (a) Diurnal cycle of freshwater flux anomalies (evaporation minus precipitation, gray) and the cumulative freshwater fluxes (red) averaged over all data collocated with drifter measurements. (b) Diurnal cycles of evaporation (blue) and precipitation (black) from MERRA-2, and evaporation anomalies projected from the diurnal temperature observed by drifters at 0.2 m (green). (c) Diurnal cycle of salinity at 0.2 m depth observed from drifters (black), induced by MERRA-2 freshwater fluxes (red), induced by MERRA-2 evaporation (blue), and induced by MERRA-2 evaporation plus evaporation anomalies projected from the diurnal temperature observed by drifters at 0.2 m (green). Correlations of the projected salinities with the observed salinity (black) are included with the corresponding colors. Shading indicates two standard errors.

its phase mirrors exactly the surface temperature diurnal cycle with maximum at 15:00 and minimum at 7:00 (Figure 13b). As noted before, MERRA-2 does not resolve the surface temperature diurnal cycle; therefore, these temperature-induced diurnal anomalies in evaporation ΔE are likely missing in the MERRA-2 evaporation.

The diurnal cycle of salinity is rather noisy (Figure 12b) with larger uncertainties. Nevertheless, salinity at 0.2 m depth experiences a statistically significant diurnal cycle with peak-to-peak amplitude of 0.005 psu, which constitutes half of the value found in the tropics at 1 m depth [*Cronin and McPhaden*, 1999]. Figure 12b shows that diurnal anomalies in $S_{0.2m}$ are positive from early morning (08:00 local time) to late afternoon (17:30) and negative from 18:00 to 07:30 on the next day. $S_{0.2m}$ reaches its diurnal maximum around 13:00. This is consistent with the diurnal variations in freshwater fluxes (evaporation minus precipitation), which are mostly controlled by evaporation in this region (Figures 13a and 13b). The precipitation is rather noisy and does not show a statistically significant diurnal cycle. The impact of diurnal wind anomalies (ΔU) on evaporation is evaluated using a similar equation as before, $\Delta E = \rho_a C_D \Delta U (q_s - q)$, and constant values for other parameters. Results indicate that wind accounts for 67% of the diurnal variance in MERRA-2 evaporation.

Figure 13a shows the anomalous diurnal freshwater flux and the cumulative flux. The positive anomalies in cumulative flux and their peak hour match well those in $S_{0.2m}$. Assuming that the freshwater flux anomalies are well mixed in the upper 0.2 m layer, the freshwater flux-induced salinity anomalies $[S(t) = S(0) + \int_0^t \frac{(E-P)S}{h} dt, where\ h = 0.2\ \text{m}]$ well capture the observed increase of salinity from 06:00 to 13:00 (Figure 13c). The observed salinity decrease afterward is much weaker than that projected from the freshwater flux anomalies. The projected salinity from evaporation alone better matches the observed diurnal cycle (Figure 13c). As mentioned earlier, the surface diurnal temperature induced-evaporation is missing in MERRA-2. Adding the diurnal anomalies of evaporation ΔE from our simple calculation to the evaporation from MERRA-2, the agreement between the projected salinity and the observed diurnal cycle of $S_{0.2m}$ is further improved (green and black curves in Figure 13c). At 5 m depth the diurnal variations in salinity are very weak. The diurnal anomalies of S_{5m} are not significantly different from zero, except for the weak positive anomalies around 12:30–15:00 (Figure 12b).

Previous studies [e.g., *Clayson and Weitlich*, 2005; *Kawai and Wada*, 2007; *Gille*, 2012; *Weihs and Bourassa*, 2014] have shown that the diurnal cycle in temperature changes seasonally and with latitude. The majority of the drifter measurements are centered around 20°S and 25°S. Although one drifter was deployed farther north at 8.8°S and then drifted to 25°S, it is difficult to examine the latitudinal dependence of the diurnal cycle because of the changes in observational time and the potential seasonality in the diurnal cycle. The longer-term measurements at 20°S and 25°S do not show a significant difference in diurnal cycle. Monthly averages of the drifter measurements reveal seasonal variations in the amplitude of the diurnal cycle of temperature at both depths (Figure 14a). The amplitude is large during austral summer, with a maximum in

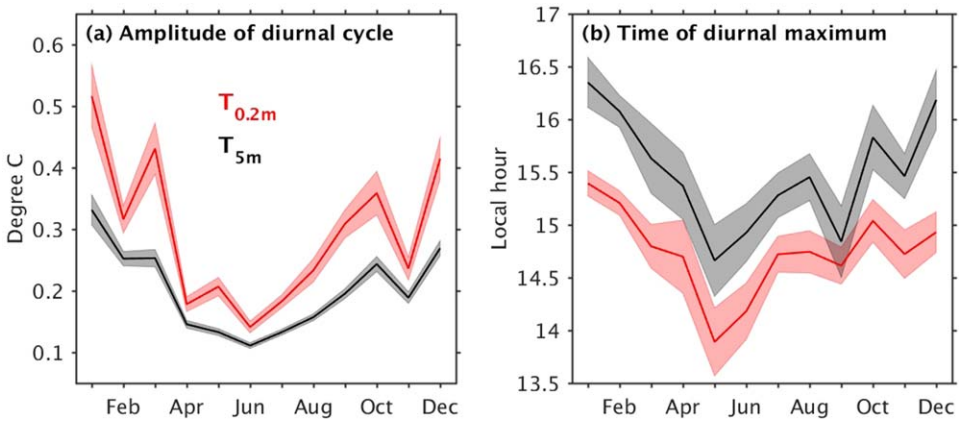

Figure 14. Seasonal variations in the amplitude (a) and the timing of the diurnal maximum (b) for temperature at 0.2 m depth (red) and 5 m depth (black). The shading shows two standard errors for the corresponding variables.

January of about 0.52°C at a depth of 0.2 m and 0.34°C at 5 m. The minimum occurs in June, with amplitudes of 0.15 and 0.12°C for 0.2 m and 5 m, respectively. As expected, the amplitude at 0.2 m depth is always larger than that at 5 m depth, and the difference in amplitude between the two depths tends to be smaller during austral winter months and larger during austral summer months. Interestingly, the monthly averages also show seasonal variations in the timing of the diurnal maximum (Figure 14b). At 0.2 m depth, during January–February temperature reaches its diurnal maximum about 0.5–1.0 h later than the average peak hour of 14:45. In contrast, during May–June the temperature maximum occurs 0.5–1.0 h earlier than the average. Similarly, T_{5m} also reaches its diurnal maximum at an earlier time during May–June and at a later time during December–February. The temperature at 5 m depth always reaches its maximum at a later time compared to the temperature at 0.2 m, although the delay time during April–July is not statistically significant. The seasonality of the amplitude and timing of the diurnal cycle are mainly due to seasonal variations of the solar radiation and wind speed, which are discussed in detail in the following section.

4.2. Influence of Wind Speed and Solar Radiation on Diurnal Cycle

Wind speed strongly influences the diurnal cycle of temperature [e.g., *Fairall et al*., 1996; *Kawai and Wada*, 2007; *Gentemann et al*., 2009]. Drifter data indicate that the strongest impact is on the amplitude of the diurnal cycle at 0.2 m depth. Figure 15a shows the amplitude of the diurnal cycle versus wind speed. The daily averages of wind speed from MERRA-2 are used, and the diurnal amplitudes are averaged within each 0.5 m/s wind speed band. The amplitude decreases rapidly from 1.44°C at 1.5 m/s wind to 0.22°C at 6 m/s wind, then decreases slowly to 0.11°C at 10 m/s wind. Although the amplitudes of the diurnal cycle at 5 m depth are not statistically different for wind speeds below 3 m/s, the amplitude shows a peak of 0.44°C at 1.5 m/s wind. The amplitude decreases to 0.11°C for 10 m/s wind. For wind speeds above 6 m/s, the amplitudes at 5 m are not statistically different from those at 0.2 m, suggesting again that the water column is well mixed for higher wind conditions. The decrease of the amplitude at both depths toward lower winds below 1.5 m/s is probably due to the fact that the limited cases observed with low-wind condition are all during austral winter (June–August) when the solar insolation is low and the diurnal warming is weak. Only 3 days with daily average wind close to 1 m/s were observed, and the solar insolation during these 3 days is below average. Of course, this decrease could also be due to noise in the data.

Another strong effect of wind speed is its impact on the timing of the maximum diurnal temperature at 5 m depth, though it has little impact on the timing of maximum diurnal temperature at 0.2 m. Figure 15b shows the times of diurnal maxima against wind speed, derived in the same way as for the amplitude of the diurnal cycle. In general, $T_{0.2m}$ reaches its diurnal maximum around 14:30–15:00 local time, with a slight delay for winds lower than 3 m/s. Diurnal maxima in T_{5m} occur later than that in $T_{0.2m}$ for winds below 9 m/s. The time of the diurnal maximum of T_{5m} increases from 15:00 to 17:50 with decreasing wind speed. With 1 m/s winds, the temperature maximum at 5 m occurs about 3 h later than that at 0.2 m depth. The delay time of temperature maxima between 5 m and 0.2 m depths decreases with increasing wind, to about half an hour for winds above 6 m/s.

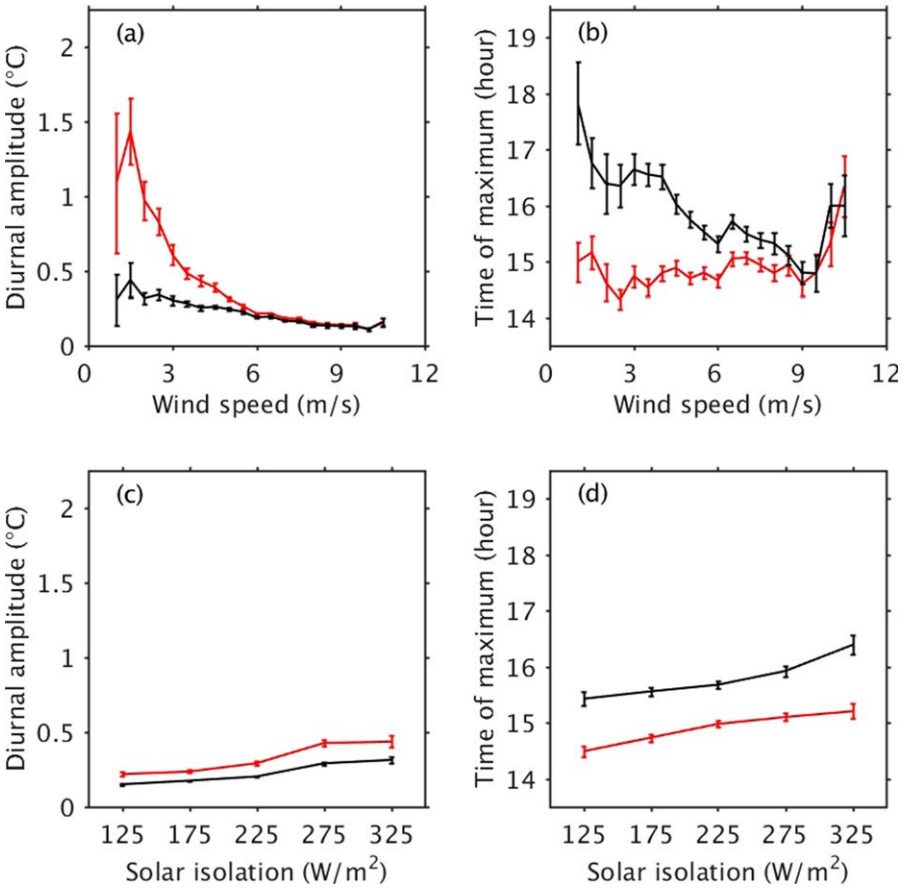

Figure 15. Changes of (a) the amplitude of diurnal cycle and (b) the timing of diurnal maximum with wind speed for temperature at 0.2 m depth (red) and 5 m depth (black), respectively. Changes of (c) the amplitude of diurnal cycle and (d) the timing of diurnal maximum with solar insolation at 0.2 m (red) and 5 m (black). Vertical bars indicate two standard errors.

The amplitude and timing of the diurnal cycle in temperature are also influenced by solar insolation, although the impact is not as strong as for wind speed (Figures 15c and 15d). Following the same procedure as for wind speed, the daily averages of solar insolation from MERRA-2 are used, and the diurnal amplitudes are averaged within each 50 W/m^2 band. The diurnal amplitude for $T_{0.2m}$ increases with increasing solar insolation, from 0.24 to 0.47°C as solar insolation increases from 125 to 325 W/m^2. The increase in diurnal amplitude at 5 m depth with solar insolation is slightly weaker, from 0.15 to 0.34°C. The time of day of the temperature maximum also increases with increasing solar insolation at both depths (Figure 15d), meaning that the temperature reaches its diurnal maximum at a later time with higher solar insolation. The time delay is about half an hour for $T_{0.2m}$ (from 14:30 to 15:00), and an hour for T_{5m} (15:30 to 16:30). This time delay is due to the longer warming duration when the solar insolation is strong.

A similar analysis of the dependence of the diurnal amplitude of salinity on wind indicates that near-surface salinity experiences a statistically significant diurnal cycle only when the wind speed is less than 6 m/s (Figure 16). The diurnal amplitude of salinity shows a large decrease as the winds increase from 1 to 3 m/s, and the amplitudes for cases with winds between 3 and 6 m/s are marginal. There are 26 days with daily average wind speed no greater than 2 m/s during our observations. The diurnal cycle averaged during those days gives an amplitude of 0.10 psu (Figure 16b), an order of magnitude larger than the overall average. Those low-wind events do not show a strong seasonal dependence. Averages of salinity for winds between 2 and 4 m/s give a diurnal amplitude of 0.02 psu. For those cases with winds below 4 m/s, the diurnal cycle is consistent with salinification driven by weak mixing under low-wind conditions (Figure 16b). The marginal diurnal cycle for winds above 4 m/s but below 6 m/s may be due to rainfall-induced freshening at the surface (Figure 16b). We have also examined the dependence of the diurnal cycle in salinity on freshwater flux, however, probably because of the impact of wind, we did not find a robust relationship.

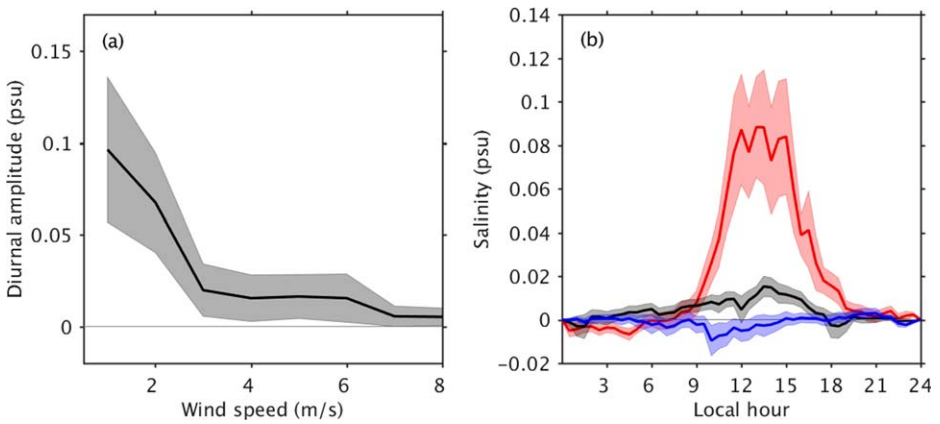

Figure 16. (a) Changes of the amplitude of diurnal cycle in $S_{0.2m}$ with wind speed. (b) Averaged diurnal variations of $S_{0.2m}$ depth for cases with wind speed $\leq$2 m/s (red), cases with wind speed between 2 and 4 m/s (black), and cases with wind speed between 4 and 6 m/s (blue). Shadings indicate two standard errors.

Overall, consistent with *Asher et al*. [2014], our results suggest that the diurnal salinification is unlikely to result in significant biases in satellite salinity retrieval. Even under weak wind conditions, the diurnal amplitude of 0.1 psu is below the accuracy of the current satellite missions. Therefore, at this time, the diurnal salinification is not a concern for satellite salinity retrieval algorithms.

5. Summary and Discussion

The 17 month long measurements in the subtropical South Pacific from three dual-sensor drifters deployed in 2015 show that the time-mean salinity difference between 0.2 and 5 m depths is very small (-0.013 ± 0.002 psu). This suggests that the salinity differences between the gridded products from Argo floats and Aquarius in this region are not due to surface salinity stratification. However, this does not necessarily mean that the differences come from the uncertainties in satellite retrievals. The differences in spatial and temporal sampling as well as in the optimal interpolation schemes could also account for the salinity differences between Argo and Aquarius gridded maps. The time-mean temperature difference between the two measurement depths is also very small but positive because of diurnal warming (0.024 ± 0.004°C).

Although the mean difference between the two depths is small, large salinity and temperature differences between the two depths occur quite often during events with strong rainfall or low-wind speed. The drifter measurements show the expected near-surface freshening and cooling during rainfall events, with the largest freshening and cooling exceeding -1.6 psu and -0.8°C, respectively. However, the relationship between the magnitude of freshening/cooling and the strength of rainfall is nonlinear, mostly due to the impact of winds, though the errors in MERRA-2 product could also deteriorate the relationship. The near-surface freshening/cooling and vertical gradient can be very small during heavy rain events with strong winds that rapidly mix the freshwater input over a thicker layer. In contrast, light rain events with weak winds can induce strong surface freshening/cooling and large vertical gradients. A near-surface haline layer down to at least 0.2 m is also observed when the surface warming is strong and the wind is weak. This haline layer is likely due to weak mixing under low winds, which confines evaporation-induced salinification in a thin layer. The largest salinity difference between the two depths (0.2 and 5 m) during the study period is about 0.56 psu. The concurrent response of the temperature and salinity to rainfall and low-wind events results in a significant positive correlation between salinity differences and temperature differences between the two measurement depths. For warming cases, the relationship is more robust with a 1°C temperature difference corresponding to a salinity difference of 0.05 psu. However, for cooling cases, although statistical analysis suggests that a 1°C temperature difference corresponds to 2.20 psu salinity difference, the relationship is much noisier.

Despite the apparent correspondence of the surface freshening to the occurrence of rain events, no simple linear relationship between ΔS ($S_{0.2m} - S_{5m}$) and the rain rate or 12 h cumulative rain was found in our study region. This is mainly due to the impact of wind on surface mixing. Using the Generalized Ocean Turbulence

Model (GOTM) *Drushka et al*. [2016] suggested that the maximum ΔS between 0.1 and 5 m (ΔS_{max}) during rain events can be parameterized as a function of maximum rain rate (R_{max}) and wind speed (U), $\Delta S_{max} = AR_{max}U^{-b}$, with $A = -0.11 \pm 0.03$ psu/(mm/h) and $b = 1.1 \pm 0.03$. Applying this relationship to the drifter and MERRA-2 data, the predicted ΔS_{max} for the observed freshening cases from drifters are usually weaker than the measured ΔS_{max}, in particular for low-wind cases in which predicted ΔS_{max} can be an order of magnitude smaller than the measured value. Possibly this is because the freshening process measured by drifters is different from those measured from mooring and ship-mounted instruments, which were used to validate the GOTM simulations. The freshening events presented in *Drushka et al*. [2016] had a typical duration of less than 2 h, whereas those observed from drifters are longer, with the freshening often lasting 12 h to 1 day. In addition, the Lagrangian measurements from the drifters tend to follow the fresh puddles and, therefore, can better track the fate of freshwater input. In addition, the extreme values in rainfall and wind may not be well represented in MERRA-2 data due to spatial and temporal averaging.

The half-hourly data also reveal interesting diurnal variability of temperature and salinity. Temperatures at both depths experience a diurnal cycle, whereas a diurnal cycle in salinity is only observed at 0.2 m depth. It is well know that the diurnal cycle in temperature is driven by diurnal solar heating, but the magnitude of diurnal heating is largely influenced by the surface wind condition. The amplitude of the diurnal cycle in $T_{0.2m}$ decreases rapidly with increasing wind speed up to 6 m/s. The amplitude of the diurnal cycle in T_{5m} also decreases with increasing wind, but at a much weaker pace. Although wind has little impact on the time of diurnal maximum in $T_{0.2m}$, it has a strong impact on the time of diurnal maximum in T_{5m}. The peak time in T_{5m} delays gradually with decreasing wind speed. Solar insolation also impacts the amplitude and phase of the diurnal cycle of both $T_{0.2m}$ and T_{5m}. At both depths, the amplitude of the temperature diurnal cycle increases and the time of the diurnal maximum delays with increasing solar insolation.

The amplitude of the diurnal cycle of salinity at 0.2 m depth (0.005 psu) is about half of that found in the tropical regions at 1 m depth. The phase of the salinity diurnal cycle is consistent with the diurnal changes in the freshwater anomalies. However, unlike in the tropics where precipitation dominates [*Cronin and McPhaden*, 1999], diurnal variations in the freshwater fluxes in our study region are controlled by evaporation. The diurnal cycle in surface salinity mainly occurs when surface winds are no greater than 2 m/s. Significant but marginal diurnal cycles are found for winds between 3 and 6 m/s.

Finally, we note that the relationships of surface stratification in temperature and salinity with winds, freshwater fluxes, and insolation, presented in this study, to some extent are contaminated by errors in MERRA-2 product as well as by the different temporal and spatial sampling of drifter measurements and model fields. Collocated measurements are required to improve our understanding of processes that determine the near-surface stratification.

Acknowledgments
The authors thank Shaun Dolk and Mayra Pazos for their help in drifter deployments and data acquisition. The authors also thank the two anonymous reviewers for their helpful comments and suggestions. Drifter Data can be obtained upon request by contacting the corresponding author at: shenfu.dong@noaa.gov. The MERRA-2 products are freely available at https://disc.sci.gsfc.nasa.gov/daac-bin/ftpSubset2.pl. This research was carried out in part under the auspices of the Cooperative Institute of Marine and Atmospheric Studies (CIMAS), a Cooperative Institute of the University of Miami and the National Oceanic and Atmospheric Administration (NOAA), cooperative agreement NA10OAR4320143. This work was supported by the NASA Ocean Salinity Science Team (grant NNX14AI85G), by NOAA's Climate Program Office, and by the NOAA Atlantic Oceanographic and Meteorological Laboratory (AOML).

References

Anderson, J. E., and S. C. Riser (2014), Near-surface variability of temperature and salinity in the near-tropical ocean: Observations from profiling floats, *J. Geophys. Res. Oceans*, *119*, 7433–7448, doi:10.1002/2014JC010112.

Asher, W. E., A. T. Jessup, R. Branch, and D. Clark (2014), Observations of rain-induced near surface salinity anomalies, *J. Geophys. Res. Oceans*, *119*, 5483–5500, doi:10.1002/2014JC009954.

Back, L. E., and C. S. Bretherton (2005), The relationship between wind speed and precipitation in the Pacific ITCZ, *J. Clim.*, *18*, 4317–4328, doi:10.1175/JCLI3519.1.

Boutin, J., N. Martin, G. Reverdin, X. Yin, and F. Gaillard (2013), Sea surface freshening inferred from SMOS and ARGO salinity: Impact of rain, *Ocean Sci.*, *9*, 183–192, doi:10.5194/os-9-183-2013.

Boutin, J., N. Martin, G. Reverdin, S. Morisset, X. Yin, L. Centurioni, and N. Reul (2014), Sea surface salinity under rain cells: SMOS satellite and in situ drifters observations, *J. Geophys. Res. Oceans*, *119*, 5533–5545, doi:10.1002/2014JC010070.

Boutin, J., et al. (2016), Satellite and in situ salinity understanding near-surface stratification and subfootprint variability, *Bull. Am. Meteorol. Soc.*, *97*, 1391–1407, doi:10.1175/BAMS-D-15-00032.1.

Centurioni, L. R., V. Hormann, Y. Chao, G. Reverdin, J. Font, and D. K. Lee (2015), Sea surfaces salinity observations with Lagrangian drifters in the tropical North Atlantic during SPURS: Circulation, fluxes, and comparisons with remotely sensed salinity from Aquarius, *Oceanography*, *28*, 96–105, doi:10.5670/oceanog.2015.08.

Clayson, C. A., and D. Weitlich (2007), Variability of tropical diurnal sea surface temperature, *J. Clim.*, *20*, 334–352, doi:10.1175/JCLI3999.1.

Cronin, M. F., and M. J. McPhaden (1999), Diurnal cycle of rainfall and surface salinity in the western Pacific warm pool, *Geophys. Res. Lett.*, *26*, 3465–3468.

Dong, S., S. T. Gille, J. Sprintall, and C. L. Gentemann (2006), Validation of the Advanced Microwave Scanning Radiometer for the Earth Observing System (AMSR-E) sea surface temperature in the Southern Ocean, *J. Geophys. Res.*, *111*, C04002, doi:10.1029/2005JC002934.

Donlon, C. J., P. J. Minnett, C. Gentemann, T. J. Nightingale, I. J. Barton, B. Ward, and M. J. Murray (2002), Toward improved validation of satellite sea surface skin temperature measurements for climate research, *J. Clim.*, *15*, 353–369.

Donlon, C. J., et al. (2005), The GHRSST-PP product user manual, GDS-v1.5, Rep., Int. GHRSST-PP Proj. Off., Exeter, U. K.

Drucker, R., and S. C. Riser (2014), Validation of Aquarius sea surface salinity with Argo: Analysis of error due to depth of measurement and vertical salinity stratification, *J. Geophys. Res. Oceans*, *119*, 4626–4637, doi:10.1002/2014JC010045.

Drushka, K., S. T. Gille, and J. Sprintall (2014), The diurnal salinity cycle in the tropics, *J. Geophys. Res. Oceans*, *119*, 5874–5890, doi:10.1002/2014JC009924.

Drushka, K., W. E. Asher, B. Ward, and K. Walesby (2016), Understanding the formation and evolution of rain-formed fresh lenses at the ocean surface, *J. Geophys. Res. Oceans*, *121*, 2673–2689, doi:10.1002/2015JC011527.

Fairall, C. W., E. F. Bradley, J. S. Godfrey, G. A. Wick, J. B. Edson, and G. S. Young (1996), Cool-skin and warm-layer effects on sea surface temperature, *J. Geophys. Res.*, *101*, 1295–1308.

Fore, A. G., S. H. Yueh, W. Tang, B. Stiles, and A. K. Hayashi (2016), Combined active/passive retrievals of ocean vector wind and sea surface salinity with SMAP, *IEEE Trans. Geosci. Remote Sens.*, *54*, 7396–7404, doi:10.1109/TGRS.2016.2601486.

Gentemann, C. L., and P. J. Minnett (2008), Radiometric measurements of ocean surface thermal variability, *J. Geophys. Res.*, *113*, C08017, doi:10.1029/2007JC004540.

Gentemann, C. L., F. J. Wentz, C. A. Mears, and D. K. Smith (2004), In situ validation of Tropical Rainfall Measuring Mission microwave sea surface temperatures, *J. Geophys. Res.*, *109*, C04021, doi:10.1029/2003JC002092.

Gentemann, C. L., P. J. Minnett, and B. Ward (2009), Profiles of ocean surface heating (POSH): A new model of upper ocean diurnal warming, *J. Geophys. Res.*, *114*, C07017, doi:10.1029/2008JC004825.

Gille, S. T. (2012), Diurnal variability of upper ocean temperatures from microwave satellite measurements and Argo profiles, *J. Geophys. Res. Oceans*, *117*, C11027, doi:10.1029/2012JC007883.

Gordon, A. L., and C. F. Giulivi (2008), Sea surface salinity trends over fifty years within the subtropical North Atlantic. *Oceanography*, *21*(1), 20–29.

Grodsky, S. A., J. A. Carton, and H. Liu (2008), Comparison of bulk sea surface and mixed layer temperatures, *J. Geophys. Res.*, *113*, C10026, doi:10.1029/2008JC004871.

Hodge, B. A., and D. M. Fratantoni (2014), AUV observations of the diurnal surface layer in the North Atlantic salinity maximum, *J. Phys. Oceanogr.*, *44*, 1595–1604, doi:10.1175/JPO-D-13-0140.1.

Hormann, V., L. R. Centurioni, and G. Reverdin (2015), Evaluation of drifter salinities in the subtropical North Atlantic, *J. Atmos. Oceanic Technol.*, *32*, 185–192, doi:10.1175/JTECH-D-14-00179.1.

Huffman, G. J., et al. (2007), The TRMM Multisatellite Precipitation Analysis (TMPA): Quasi-global, multiyear, combined-sensor precipitation estimates at fine scales, *J. Hydrometeorol.*, *8*, 38–55, doi:10.1175/JHM560.1.

Kawai, Y., and A. Wada (2007), Diurnal sea surface temperature variation and its impact on the atmosphere and ocean: A review, *J. Oceanogr.*, *63*, 721–744.

Kerr, Y. H., et al. (2010), The SMOS mission: New tool for monitoring key elements of the global water cycle, *Proc. IEEE*, *98*, 666–687, doi:10.1109/JPROC.2010.2043032.

Lagerloef, G., et al. (2008), The Aquarius/SAC-D mission: Designed to meet the salinity remote-sensing challenge, *Oceanography*, *21*, 68–81.

Lagerloef, G., H.-Y. Kao, T. Meissner, and J. Vazquez (2015), Aquarius Salinity Validation Analysis; Data Version 4.0, NASA Jet Propulsion Laboratory, Pasadena, Calif. [Available at ftp://podaac.jpl.nasa.gov/allData/aquarius/docs/v4/AQ-014-PS-0016_AquariusSalinityDataValidationAnalysis_DatasetVersion4.0and3.0.pdf.]

Meissner, T., F. Wentz, J. Scott, and K. Hilburn (2014), Upper ocean salinity stratification and rain freshening in the tropics observed from Aquarius, in *IEEE International Geoscience and Remote Sensing Symposium (IGARSS)*, pp. 5111–5114, IEEE, Quebec City, Canada.

Melnichenko, O., P. Hacker, N. Maximenko, G. Lagerloef, and J. Potemra (2016), Optimum interpolation analysis of Aquarius sea surface salinity, *J. Geophys. Res. Oceans*, *121*, 602–616, doi:10.1002/2015JC011343.

Molod, A., L. Takacs, M. Suarez, and J. Bacmeister (2015), Development of the GEOS-5 atmospheric general circulation model: Evolution from MERRA to MERRA2, *Geosci. Model Dev.*, *8*, 1339–1356, doi:10.5194/gmd-8-1339-2015.

Murray, M. J., M. R. Allen, C. J. Merchant, A. R. Harris, and C. J. Donlon (2000), Direct observation of the skin-bulk SST variability, *Geophys. Res. Lett.*, *27*, 1171–1174.

Raymond, D. J., S. Sessions, A. Sobel, and Z. Fuchs (2009), The mechanics of gross moist stability, *J. Adv. Model. Earth Syst.*, *1*, 20, doi:10.3894/james.2009.1.9.

Reverdin, G., et al. (2014), Validation of salinity data from surface drifters, *J. Atmos. Oceanic. Technol.*, *31*, 967–983, doi:10.1175/JTECH-D-13-00158.1.

Rhein, M., et al. (2013), Observations: Ocean, in Climate Change 2013: The Physical Science Basis. Contributions of Working Group I to the Fifth Assessment Report of the Intergovernmental Panel on Climate Change, edited by T. F. Stockeret al., pp. 255–315, Cambridge Univ. Press, Cambridge, U. K.

Roemmich, D., and J. Gilson (2009), The 2004–2008 mean and annual cycle of temperature, salinity, and steric height in the global ocean from the Argo Program, *Prog. Oceanogr.*, *82*, 81–100.

Stommel, H., K. Saunders, W. Simmons, and J. Cooper (1969), Observations of diurnal thermocline, *Deep Sea Res., Part I*, *16*, suppl., 269–284.

Volkov, D. L., S. Dong, G. Goni, R. Lumpkin, and G. Foltz (2017), Near-surface temperature and salinity stratification as observed with dual-sensor Lagrangian drifters deployed during SPURS-2 field campaign, *Geophys. Res. Abstr.*, *EGU2017–10975*, vol. 19, EGU General Assembly.

Weihs, R. R., and M. A. Bourassa (2014), Modeled diurnally varying sea surface temperatures and their influence on surface heat fluxes, *J. Geophys. Res. Oceans*, *119*, 4101–4123, doi:10.1002/2013JC009489.

Wick, G. A., W. J. Emery, L. H. Kantha, and P. Schlussel (1996), The behavior of the bulk-skin sea surface temperature difference under varying wind speed and heat flux, *J. Phys. Oceanogr.*, *26*, 1969–1988.

Yu, L. (2010), On sea surface salinity skin effect induced by evaporation and implications for remote sensing of ocean salinity, *J. Phys. Oceanogr.*, *40*, 85–102, doi:10.1175/2009JPO4168.1.

Zhang, Y., and X. Zhang (2012), Ocean haline skin layer and turbulent surface convection, *J. Geophys. Res.*, *117*, C04017, doi:10.1029/2011JC007464.